Pushing the Auger limit: Kinetics of excitons in traps in Cu_2O

D. W. Snoke and V. Negoita
Department of Physics and Astronomy, University of Pittsburgh, 3941 O'Hara Street, Pittsburgh, Pennsylvania 15260
(Received 16 September 1999)

We have measured the Auger recombination rate for excitons in Cu_2O trapped in harmonic potential wells created by inhomogeneous stress. The rate is higher than assumed in most previous experiments, but consistent with the rate reported recently by O'Hara *et al.* [Phys. Rev. B (to be published)]. We find that even given this rate, the orthoexciton density immediately after creation in the well by a short laser pulse may be high enough for Bose condensation, and there is some evidence that this may occur.

I. INTRODUCTION

The semiconductor Cu_2O is an ideal system for studying excitonic effects because of the large binding energy of the excitons (150 meV), which allows them to exist at room temperature,[1] and because of the overall repulsive interaction between the excitons, which prevents the formation of electron-hole liquid. As amply discussed elsewhere (e.g., Ref. 2), the luminescence from the two lowest exciton levels, the triplet ''orthoexciton'' and the singlet ''paraexciton,'' directly reveals the instantaneous spatial distribution and kinetic-energy spectrum of these two species of excitons. Over the past ten years, there have been several fascinating experiments done with excitons in the semiconductor Cu_2O which have indicated statistical effects related to the boson nature of the excitons and possibly Bose-Einstein condensation of excitons.[3–10]

All of these experiments have involved high-intensity excitation of the surface of bulk samples of Cu_2O, either single-photon excitation with green light[3–8] or two-photon excitation with infrared light.[9,10] In each case, the photons were absorbed within a few microns of the surface, creating a highly nonequibrium, localized gas of excitons which expanded into the crystal very rapidly. This led to (1) a very distinctive shape of the orthoexciton spectrum[3–5] which could be fit to a nearly-ideal Bose-Einstein distribution over a wide range of densities, (2) extremely fast expansion out of the excitation region,[4,7,8] and (3) anomalous paraexciton spectra.[4,6] Although the luminescence spectra could be well fit by the nearly-ideal Bose-Einstein distribution function over a wide range of density and temperature, and the density deduced from the ideal Bose gas fit scaled properly with time-resolved measurements of the exciton volume,[3] the interpretation of the spectral data was open to question because the luminescence was integrated over a volume with very inhomogeneous density, and there was no way to determine the exact distribution of densities in the micron-depth excited region near the surface. Recently, measurements of the absolute density of the excitons using calibrated photon counting[11] have indicated that the densities of the excitons in the surface-excition experiments are much less than the values indicated by the nearly ideal Bose gas fits of the spectral line shapes, and therefore the spectral line shapes must be strongly affected by the nonequilibrium, inhomogeneous distribution of the excitons. This conclusion calls into question the interpretation of many of the experiments which indicated Bose-Einstein statistics and Bose-Einstein condensation with single-photon surface excitation, although it does not directly affect the interpretation of the two-photon-excitation experiments.[9,10] The results of those experiments are consistent with the interpretation that when a laser is tuned to one half the orthoexciton ground-state energy, the excitons created in a small region of phase space near the ground state have inhibited out-scattering due to the boson nature of the excitons. Even well after the laser pulse, the sharp spectral peak created at low kinetic energy remained much longer than the exciton-phonon scattering time measured at lower density. Because the excitons were placed into low-energy states ''by hand,'' normal equilibrium considerations do not apply, and the total exciton density could be well below the critical density for equilibrium Bose-Einstein condensation. Similar results have been seen for two-photon resonant excitation of biexcitons in CuCl.[12,13] The spatial expansion measurements in Cu_2O have also been subject to differing interpretations because of the strongly nonequilibrium nature of the system; in particular, hot phonons emitted by the excitons can create a ''phonon wind'' which pushes the excitons at the speed of sound into the crystal.[14,15]

Because of the ambiguity of the surface-excitation experiments, it is appealing to create excitons in a harmonic potential trap of well-defined volume, analogous to the traps used for Bose-Einstein condensates of alkali gases,[16,17] instead of in an undefined volume at the surface. This method of trapping excitons was explored before in Cu_2O,[18] but the density of excitons in the well was never high enough for Bose-Einstein condensation, mainly because of the Auger recombination process for excitons is Cu_2O which causes a sublinear increase of the exciton density with laser power. In this process, two excitons collide, causing one of them to recombine while the other one ionizes, taking the energy of the exciton which recombined. Recent measurements of the rate of this process[19] have indicated that this is a more severe limit to the exciton density than previously thought. The recent measurements yielded a density-dependent recombination rate of $1/\tau = An$, where n is the exciton density and $A \simeq 10^{-16}$ cm^3/ns, which implies a cross section of about 1000 Å^2, compared to a collision cross section of about 5000 Å^2,[20] i.e., about one-fifth of all exciton-exciton collisions lead to recombination and ionization. In our experiments we have created excitons in a trap in Cu_2O using

high-intensity, picosecond laser pulses from a cavity-dumped, synchronously pumped dye laser tuned to the orthoexciton absorption resonance, in contrast to the quasi-cw laser excitation used in previous experiments.[18] Our primary goal has been to independently measure the Auger recombination rate to determine if it strictly prevents the excitons from reaching the critical density for Bose-Einstein condensation. To this end, we have recorded the spatial profile and total luminescence intensity of both the orthoexcitons and paraexcitons with a subnanosecond time resolution following the laser pulse. The comparison of the orthoexciton and paraexciton luminescence allows us to accurately model the interspecies conversion, while the short, intense, wavelength-tunable laser pulses allow us to reach high exciton densities at low temperatures. We have found that with our laser power, we can apparently just reach the threshold for Bose-Einstein condensation, and we have recorded spatial distributions of the excitons at high density which show behavior indicative of Bose-Einstein condensation.

II. CREATING THE TRAP

The method of using stress to create a harmonic potential inside a bulk semiconductor has been discussed at length before,[18,21] so here we give just a brief summary of the considerations. Applied stress has two main effects on the exciton energies. First, a hydrostatic stress causes an overall blue shift of the exciton energies. Second, a shear (traceless) stress changes the local symmetry, thereby causing a splitting of the valence bands. Waters *et al.*[22] calculated this splitting, using second-order perturbation theory on the basis of the 12 exciton states formed from the two Γ_6 conduction-band states and the two Γ_7 and four Γ_8 valence band states to successfully fit the energy shifts of the exciton lines under uniaxial stress. Their results for the lowest exciton energy states, namely, the paraexciton and orthoexciton states of the ''yellow'' exciton formed from the two Γ_6 conduction band states and two Γ_7 valence states, in the case of a cylindrically symmetric stress along (100), are

$$E_p = a(S_{11}+2S_{12})\sigma - \frac{18b^2(S_{11}-S_{12})^2}{\Delta}\tau^2,$$

$$E_o^{\text{doublet}} = a(S_{11}+2S_{12})\sigma - \frac{4b(S_{11}-S_{12})J}{\Delta}\tau - \frac{18b^2(S_{11}-S_{12})^2}{\Delta}\tau^2, \quad (1)$$

$$E_o^{\text{singlet}} = a(S_{11}+2S_{12})\sigma + \frac{8b(S_{11}-S_{12})J}{\Delta}\tau - \frac{18b^2(S_{11}-S_{12})^2}{\Delta}\tau^2,$$

where a is the hydrostatic deformation potential and b is the shear deformation potential, $\sigma=\sigma_{zz}+\sigma_{xx}+\sigma_{yy}$ is the hydrostatic stress and $\tau=\sigma_{zz}-\frac{1}{2}\sigma_{xx}-\frac{1}{2}\sigma_{yy}$ is the shear stress, and S_{11} and S_{12} are elastic compliance constants.

TABLE I. Parameters used in the stress calculation for Cu_2O.

Parameter	Value	References
a	1.7 eV	22–24
b	0.3 eV	22,24
S_{11}	4.169×10^{-12} cm^2/dyn	25
S_{12}	-1.936×10^{-12} cm^2/dyn	25
E_{100}	12.3×10^{11} cm^2	25
ν_{100}	0.465	25
J	22.7 meV	22
Δ	74 meV	22

Δ is the spin-orbit splitting of the valence band, and J is the spin-exchange constant. The values of the deformation potentials and the other parameters have been found from various hydrostatic and uniaxial stress measurements, and are given in Table I.

For a round stressor in contact with a planar surface of the semiconductor crystal, pressing along (100), the distribution of stresses along the axis of symmetry can be found analytically, from the solution of the ''Hertz contact problem,''[26,21] as

$$\sigma_{zz} = \frac{q_0}{1+(z/r_0)^2},$$

$$\sigma_{xx}=\sigma_{yy}=q_0\left[(1+\nu_1)\{1-(z/r_0)\tan^{-1}(r_0/z)\} - \frac{1}{2(1+(z/r_0)^2)}\right], \quad (2)$$

where r_0 is the radius of the circular contact, and q_0 is the pressure at the center of the stressor on the surface. The values of r_0 and q_0 are given by

$$r_0 = \left[\frac{3\pi}{4}FR\left(\frac{1-\nu_1^2}{\pi E_1}+\frac{1-\nu_2^2}{\pi E_2}\right)\right]^{1/3},$$

$$q_0 = \frac{3F}{2\pi r_0^2}, \quad (3)$$

where ν_1 and ν_2 are the two Poisson's ratios of the materials in contact, and E_1 and E_2 are the two Young's moduli. F is the applied force, and R is the radius of the curved stressor. Figure 1 shows the calculated energies of the paraexciton and doublet orthoexciton states as a function of depth in the crystal below the stressor contact. The singlet orthoexciton which is split off shifts upward and does not have a potential minimum. As seen in this figure, the depth and the effective force constant of the potential minima are different for the paraexcitons and orthoexcitons—the force constant for the paraexcitons is about a factor of 2 less. Also, the position of the minimum is slightly different in the two cases, by about 5 μm, because the hydrostatic stress component, which causes the strong blueshift near the surface, has a greater relative weight in the case of the paraexcitons.

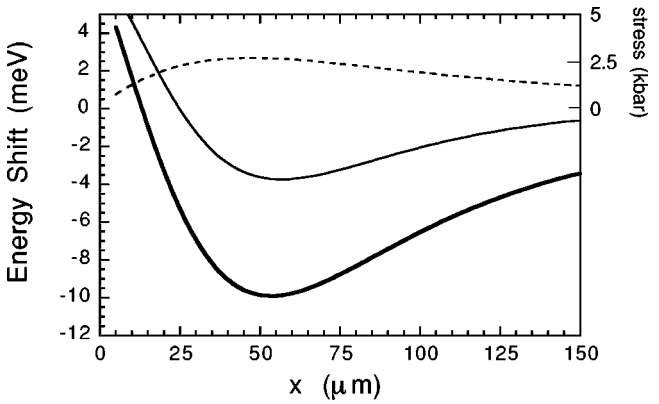

FIG. 1. Calculation of the exciton energy shift as a function of the depth x below the top of the crystal, where a curved glass stressor of radius 3 mm presses the surface with a force of 8 N. Heavy solid line: energy shift of the orthoexcitons. Thin solid line: energy shift of the paraexcitons. Dashed line: the shear stress (right axis).

Figure 2 shows two images of the luminescence from the excitons when a pure, natural-growth sample of Cu_2O is stressed in this way, as it is immersed in liquid helium at 2 K. The images were taken by projecting the image of the sample onto the entrance slit of an imaging spectrometer, which preserved the spatial information along one axis while dispersing the light along the other axis. Three lines are observed: a direct-recombination luminescence line and a phonon-assisted recombination line from the orthoexcitons, with minima at 2.024 and 2.010 eV, respectively, and a direct-recombination luminescence line from the paraexcitons with a minimum at 2.016 eV. The luminescence from the paraexcitons is forbidden along the (100) direction; therefore the sample was cut so that the viewing axis is along the (110) direction. Figure 2(a) is a time-integrated image taken as the laser spot was scanned along the stress axis. The overall shifts of the lines are consistent with the stresses obtained in the above calculation, as well as with previous measurements;[27] the shape and depth of the minima also

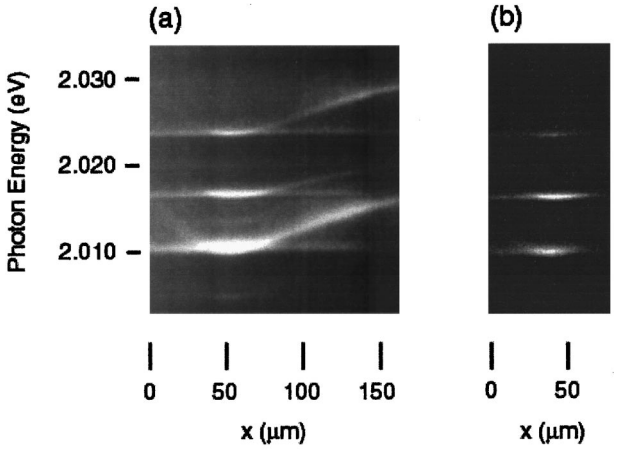

FIG. 2. (a) Time-integrated image of the exciton luminescence taken through an imaging spectrometer, as the laser is scanned along the crystal. (b) The same image when the laser is set to the position of the potential minimum instead of scanned, showing the equilibrium distributions of the excitons.

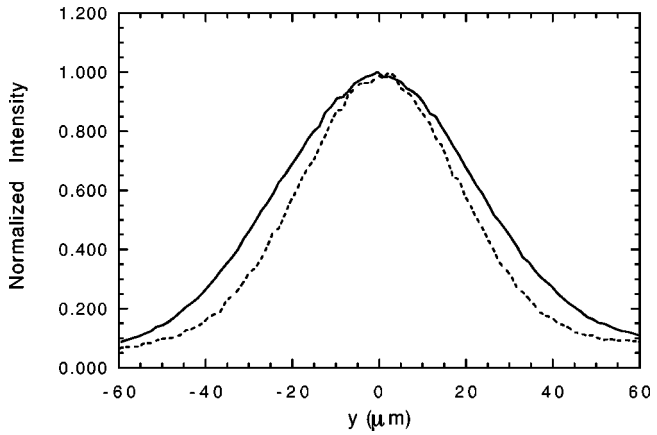

FIG. 3. Spatial profiles of the total spectrally integrated orthoexciton phonon-assisted recombination luminescence (solid line) and the paraexciton direct-recombination luminescence (dashed line) in a Cu_2O crystal at 2 K, 100 ns after a short (5 ps) laser pulse. Although the spectral shapes of these two luminescence lines are different, for a classical gas in equilibrium, the total integrated luminescence from these two lines will have the same FWHM if they are in the same harmonic potential. The difference of the widths is because they ''feel'' different harmonic potentials.

agrees with the calculation. The horizontal lines in this image come from bright luminescence which has been scattered from the crystal surfaces, giving a diffuse background. Figure 2(b) shows the luminescence taken under the same conditions, except that the laser is focused on the center of the well and is not scanned.

For classical particles in equilibrium, the volume is found by setting[18]

$$n(r)=n(0)e^{-\alpha r^2/k_BT}, \tag{4}$$

where α is the effective force constant of the potential minimum. The energy minimum of the orthoexcitons shown in Fig. 2 fits a harmonic potential with force constant of 1500 meV/mm^2. At 2 K, Eq. (4) implies a full width at half maximum (FWHM) of 18 μm for the orthoexcitons. Since the force constant of the paraexciton energy minimum is approximately half that of the orthoexcitons, the paraexciton distribution in equilibrium should be about 40% wider. Figure 3 shows measurements of the spatial profiles of the orthoexciton and paraexciton luminescence in a trap created in this way, at late times after a short (5 ps) laser pulse, when the crystal is immersed in liquid helium at 2 K. The data were taken using a transparent block to scan the image of the sample across the entrance slit of a spectrometer.[28] The direction of the scan shown in Fig. 3 is perpendicular to the stress axis, while the luminescence was integrated along the stress axis of the crystal and along the other perpendicular axis. As seen in this figure, the paraexciton cloud is 20% larger than the orthoexciton cloud, consistent with the fact that the harmonic minimum force constant for the paraexcitons is lower than that of the orthoexcitons. We note, however, that the force constant of the potential minimum is not necessarily the same in one of the two lateral directions, the direction of this scan, as it is along the x (stress) axis, and therefore the FHWM of the orthoexciton distribution at late time does not necessarily approach the value of 18 μm calculated above. While this perpedicular force constant cannot be calculated analytically, it should be on the same order as,

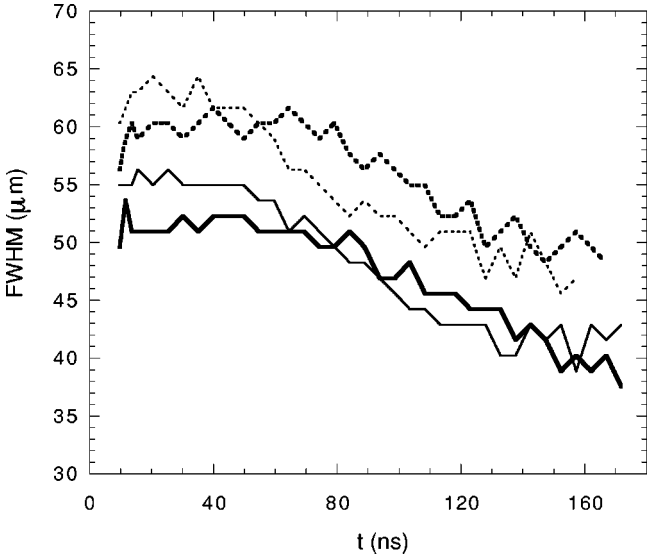

FIG. 4. Full width at half maximum of the spatial profiles of the exciton luminescence as a function of time after a short (5 ps) laser pulse. Heavy solid line: orthoexciton width following a 18-nJ laser pulse. Heavy dashed line: paraexciton width following a 18-nJ laser pulse. Thin solid line: orthoexciton width following a 6-nJ laser pulse. Thin dashed line: paraexciton width following a 6-nJ laser pulse.

but slightly lower than, the on-axis force constant, since the large hydrostatic blueshift near the crystal surface gives a stiffer force constant in that direction, as seen in Fig. 1. In the following, we will assume that the force constants in all three dimensions are the same.

III. MEASUREMENT OF THE AUGER CONSTANT

Knowing the volume of both exciton species, we can accurately estimate the exciton densities and deduce the Auger density-dependent recombination rate. Figure 4 shows the FWHM of the exciton luminescence as a function of time, when the laser photon energy is tuned to one optical phonon (the 13.6-meV Γ_{12} phonon) above the ground state of the orthoexcitons in the strain-induced trap. This allows a strong absorption of the laser photons via the phonon-assisted absorption process, and creates a large population of orthoexcitons directly in the center of the trap. Because the energy of the trap is lower than that of the surrounding medium, the laser passes through the crystal without being absorbed until it reaches the trap. As seen in this figure, the volume of both exciton species remains roughly constant for the first 50 ns and then drops, for both excitation powers. We believe that this is because phonons emitted by the excitons remain in the region, heating the exciton gas, and the temperature drops nonlinearly at late time due to the phonon-phonon interaction. As the exciton temperature drops, their volume drops, according to Eq. (4). If we restrict our attention to the first 50 ns, however, we can approximate that the volume is constant, which greatly simplifies the analysis. Figure 5(a) shows the total spatially and spectrally integrated orthoexciton luminescence as a function of time following a 6-nJ laser pulse for the same data set used in Fig. 4. Because the orthoexcitons are hot at early times, as discussed in Sec. IV, some of the orthoexciton luminescence falls outside the

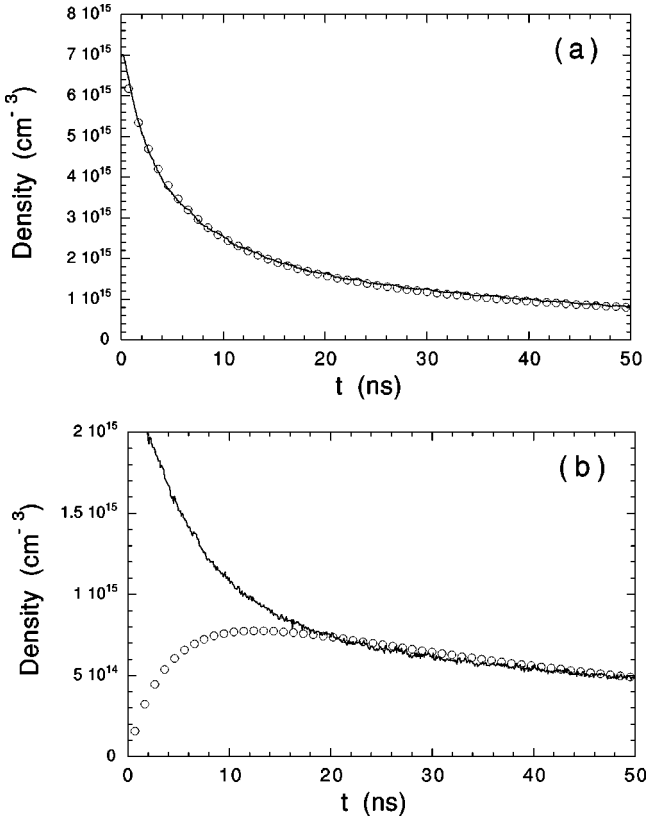

FIG. 5. (a) Total orthoexciton luminescence in the spectral range as a function of time following a short (5 ps) laser pulse of 6 nJ. (b) Total luminescence in the paraexciton spectral range. At early times hot orthoexciton luminescence dominates, while at late times it is entirely the paraexciton luminescence.

spectral range of intregration, so that this curve slightly undercounts the orthoexcitons at early times. Figure 5(b) shows the total spatially integrated luminescence in the paraexciton spectral range, 614.5–615.3 nm. The luminescence at early times is entirely from hot phonon-assisted orthoexciton luminescence. Because the orthoexcitons are cold at late times, all of the luminescence at late times in this curve comes from the paraexcitons. Figures 6(a) and 6(b) show the same curves for the case of a 18-nJ pulse. Each of these curves is fit to a solution of the rate equations for the orthoexciton density n_o and the paraexciton density n_p, given by

$$\frac{\partial n_o}{\partial t} = -A_1 n_o^2 + \frac{3}{8}(A_1 n_o^2 + A_2 n_p^2),$$
$$\frac{\partial n_p}{\partial t} = -A_2 n_p^2 + \frac{1}{8}(A_1 n_o^2 + A_2 n_p^2), \tag{5}$$

where A_1 and A_2 are the Auger constants for the orthoexcitons and paraexcitons, respectively, which in principle could be different but are found to be equal in these fits. In principle, one could also have an interspecies process involving collisions between orthoexcitons and paraexcitons, but we find that it is not necessary to invoke such a term to fit the data, and then, when such a term is introduced, the fit of the data is always worse. We have not included any temperature dependence of the Auger rates, although the temperature of the exciton gas changes substantially in the first few nano-

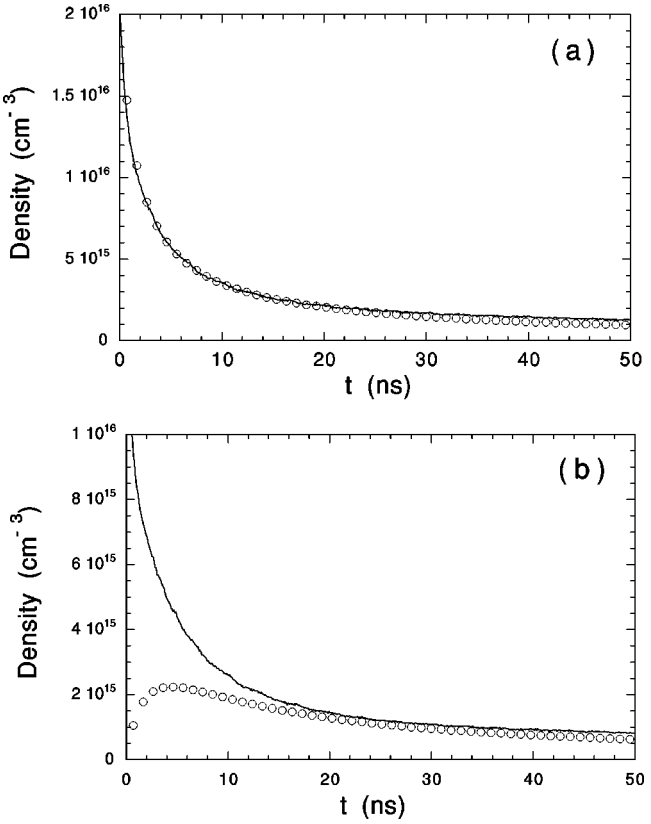

FIG. 6. The same curves as in Fig. 4 but for a 18-nJ laser pulse.

seconds after the laser pulse. The last terms on the right-hand side of both equations take into account the assumption that one-half of the affected excitons are ionized and return to the system with their spin randomized, three-fourths as orthoexcitons and one-fourth as paraexcitons. We also have not included terms for excitonic radiative recombination or density-independent, phonon-assisted ortho-para conversion. Radiative recombination is extremely slow for excitons in Cu_2O; recent estimates of the radiative lifetimes are 14 μs for the orthoexcitons and 7 ms for the paraexcitons,[11] much longer than the time scales of interest here. At temperatures of a few K, the phonon-assisted ortho-para conversion process is also expected to be very slow,[29] and the present measurements do not require such a process. As discussed below, the population of paraexcitons at late times is consistent with the above equations, which imply that all conversion of orthoexcitons to paraexcitons occurs by means of the Auger process; the rate of decay of the orthoexciton population at late time implies that the density-independent, phonon-assisted ortho-para conversion time must be much greater than 50 ns.

As seen in Figs. 5 and 6, this much-simplified model fits the orthoexciton data well over a wide range of densities. The model allows only two parameters for the fits to all four of the curves, namely, the Auger constant A and an overall multiplier for the paraexciton luminescence intensity relative to the orthoexciton intensity, which takes into account the fact that the radiative efficiencies of the orthoexcitons and paraexcitons are not the same—the paraexciton luminescence is forbidden at zero stress and increases in efficiency as the stress increases. This fit implies that the orthoexciton phonon-assisted luminescence is 2.7 times more efficient along this viewing axis than the paraexciton direct luminescence at this applied stress. To convert the photon count rate which we measure to an absolute density, we have measured the laser power incident on the sample, and estimated the absorbed fraction. We assume that all of the absorbed photons become orthoexcitons, because the paraexciton phonon-assisted absorption process is much weaker than the orthoexciton phonon-assisted absorption,[30] and the paraexciton direct absorption process is forbidden by momentum and energy conservation at this photon energy. Because of the uncertainties of measuring the absorbed laser power, we use the recorded[31] absorption spectrum for orthoexciton phonon-assisted absorption as a crosscheck, assuming that the orthoexciton phonon-assisted absorption spectrum is unchanged under stress except for a shift in energy. Knowing the absorption coefficient and the effective path length of the light through the strain well, we estimate that 5% of the laser light is absorbed in the well. For a total laser energy per pulse incident on the sample at the highest laser power of 18 nJ, with 20% reflected from the first crystal surface and 5% absorbed in the stress-induced well, we therefore deduce a total of 2×10^9 orthoexcitons created initially. The FWHM of the orthoexciton distribution at early time in the lateral direction is 50 μm, as seen in Fig. 4. This implies a volume of approximately $(50\ \mu\text{m})^3=10^{-7}\text{cm}^3$, for an initial orthoexciton density of $2\times10^{16}\text{cm}^{-3}$. The number of orthoexciton counts at $t=0$ scales linearly with the incident laser power, which implies that the initial count rate can be equated with this density. The initial lifetime of the orthoexciton luminescence at the highest density is 2 ns compared to our time resolution of about 100 ps, which means that the Auger process does not affect the initially measured intensity. The value of $A=A_1=A_2$ deduced from these fits is $1\times10^{-16}\text{cm}^3/\text{ns}$. This is consistent with the value of 7×10^{-17} reported by O'Hara *et al.*,[19] who estimated an uncertainty of a factor of 2 in their value. We estimate that our value may also be off by a factor of 2, based on the accumulated errors in the measured volume, count rate, laser power, etc. Both of these values are substantially higher than calculated theoretically,[32] and higher than estimated from previous experiments using spectral lineshape analysis.[5]

IV. BOSE-EINSTEIN STATISTICAL CONSIDERATIONS AT HIGH DENSITY

Given this calibration of the density and lifetime of the excitons, are we near the critical threshold for Bose-Einstein condensation of excitons? The measured spatial profile of the excitons acts as a thermometer of the internal temperature of the excitons, according to Eq. (4), in addition to the spectral line shapes, which depend on temperature. In Sec. II we calculated that the equilibrium distribution FWHM of the orthoexcitons along the stress axis at the helium bath temperature of 2 K was 18 μm, while the measured average FWHM of the orthoexcitons along the stress axis in Fig. 2 is 30 μm. This implies that the excitons are hotter than the liquid helium bath at early times, which is consistent with the recorded spectral shape of the phonon-assisted orthoexciton luminescence line. Although the orthoexcitons are created at low energy near their ground state by the resonantly-tuned laser, the temperature is quickly raised by the Auger

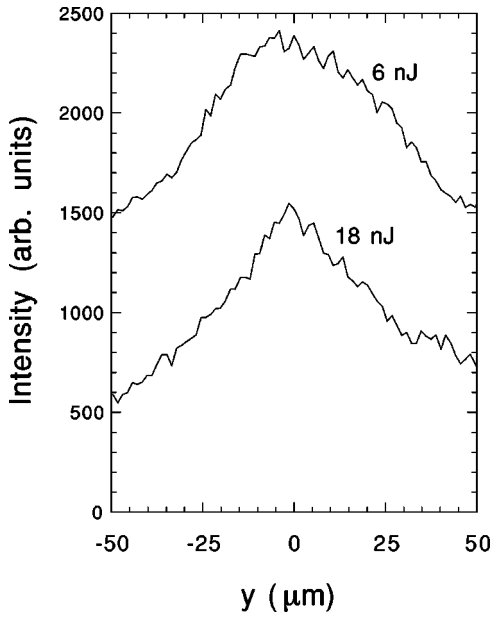

FIG. 7. Spatial profiles of the orthoexciton phonon-assisted recombination luminescence at $t=0$ during the short (5 ps) laser pulse, for two laser pulse energies, from the same data set as in Fig. 3.

process,[5] which ionizes the excitons, to about 20 K. As seen in Fig. 4, the lateral FWHM of the orthoexcitons decreases in time as the exciton gas cools toward the lattice temperature of 2 K. For an isotropic three-dimensional harmonic potential minimum, the critical number for Bose-Einstein condensation is well known, as[2]

$$N_c = 1.2g\frac{(k_B T)^3 m^{3/2}}{\hbar^3 \alpha^{3/2}}, \tag{6}$$

where m is the mass of the particles and g is the level degeneracy, equal to 2 for the orthoexcitons and 1 for the paraexcitons. For $m=2.7m_0$,[33] and the force constants deduced in Sec. II, this implies a critical number for condensation of approximately 6×10^8 at 2 K for both the orthoexcitons and paraexcitons (the paraexcitons have no level degeneracy but have a lower force constant.) At 20 K this critical number is 6×10^{11}. The total number of orthoexcitons created by the most intense laser pulse, 2×10^9, is much less than the critical number for condensation at 20 K, the temperature at early time. At late times, as the temperature of the orthoexcitons falls toward 2 K, the total number of orthoexcitons falls by a factor of 20 (with a comparable number of paraexcitons), as seen in Fig. 6. This implies that at late times the total number of excitons is around 1/10 that needed for Bose-Einstein condensation at 2 K. At very early times, however, the orthoexcitons which are created resonantly near their ground state are cold; the Auger process heats them on the same time scale as the recombination rate, i.e., in about 2 ns. During this time the number of orthoexcitons of approximately 2×10^9 in the well greatly exceeds the critical number for condensation of 6×10^8 at 2 K. Is there any evidence for Bose-einstein effects during this early period? Figure 7 shows the spatial profile of the orthoexciton luminescence at $t=0$ for the two cases used in Figs. 4–6. As seen in this figure, the profile in the high-density case has an anomalous peaked shape very similar to those seen in alkali gases in optical traps.[16,17] In the low-density case and at all lower densities, the profile is broad and Gaussian.

Although this profile is very suggestive of Bose-Einstein condensation, it is too soon to conclude that this must be the case. The highly nonequilibrium nature of the exciton gas at early time requires further study of this early stage with better time resolution. Nevertheless, it is hard to imagine other reasons for the spatial profile of the exciton gas to contract *inwardly* at high density. Normally, the Auger effect causes the temperature of the gas to increase at high density, which should make the cloud become larger. The Auger process also tends to suppress sharp features in the spatial distribution, since more dense regions decay faster.

In a way, the condensate has been placed ''by hand'' into the trap at an early time by the intense laser pulse which is tuned in wavelength near to the ground state of the orthoexcitons. We note, however, that the excitons are not created *coherently* in this state. Because the excitons are created via the phonon-assisted absorption process, which involves an incoherent phonon background, the excitons have random phase when they are created. As in the case of the alkali atoms in optical traps which are subject to recombination into molecules, there is a heirarchy of time scales; the excitons scatter with each other and emit phonons faster than they recombine via the Auger process. The results from alkali gases show that even though a recombination process removes the particles, condensation is still possible on time scales short compared to the time scale for recombination. We can therefore expect that further study of the orthoexcitons on very short time scales may confirm the Bose-Einstein nature of the early result shown in Fig. 7. There is a clear advantage to resonant creation of the orthoexcitons. The number of excitons in the well is proportional to αl, where $\alpha \propto \sqrt{E}$ is the phonon-assisted absorption constant, and $l \propto \sqrt{E}$ is the effective path length of laser beam through the well, giving $N \propto T$, while the critical number in the well is proportional to T^3.

V. CONCLUSIONS

These measurements imply that for most of the lifetime of the excitons in the traps, they are well below the critical density for Bose-Einstein condensation in the trap even for the most intense laser pulses, because of the Auger effect. This process not only causes a fast recombination of the excitons at high density but also heats up the gas, both of which effects oppose Bose-Einstein condensation. Importantly, however, these measurements indicate that at early times the number of orthoexcitons can exceed the critical number for condensation on short-time scales before the Auger process heats the exciton gas and destroys it. The spatial profile of the orthoexcitons at early time is suggestive of Bose-Einstein condensation, but further study with better time resolution is necessary to confirm this. It may also be beneficial to use higher laser power and/or to use two-photon excitation of the orthoexciton ground state. The number we obtain for the Auger recombination rate, 1×10^{-16} cm^3/ns, is consistent with the previously reported[19] value of 7

$\times 10^{-17}$ cm^3/ns, in contrast to previous estimates[5] of 10^{-18} cm^3/ns. This value has a large uncertainty due to the unavoidable uncertainties in estimating the number of excitons in the well. Despite these uncertainties, however, our simultaneous observation of the paraexciton luminescence puts tight constraints on the fits.

The trap method used here is very appealing because it creates an inward force on the excitons, preventing the ambiguities of the hyrodynamics of an expanding gas seen in previous experiments on Bose Einstein effects of excitons in Cu_2O, and allowing a telltale spatial distribution for Bose-Einstein condensation.

ACKNOWLEDGMENTS

This work was supported by the National Science Foundation as part of Early Career Award No. DMR-97-22239. One of the authors (D.S.) is a Cottrell Scholar of the Research Corporation. We thank I. Hancu for early contributions to these experiments, and H. Ray for contributions to the analysis.

[1] D. W. Snoke, A. J. Shields, and M. Cardona, Phys. Lett. B **45**, 11 693 (1992).
[2] J. P. Wolfe, J. L. Lin, and D. W. Snoke, in *Bose–Einstein Condensation*, edited by A. Griffin, D. W. Snoke, and S. Stringari (Cambridge University Press, Cambridge, 1995).
[3] D. W. Snoke, J. P. Wolfe, and A. Mysyrowicz, Phys. Rev. Lett. **59**, 827 (1987).
[4] D. W. Snoke, J. P. Wolfe, and A. Mysyrowicz, Phys. Lett. B **41**, 11 171 (1990).
[5] D.W. Snoke and J. P. Wolfe, Phys. Rev. B **42**, 7876 (1990).
[6] J. L. Lin and J. P. Wolfe, Phys. Rev. Lett. **71**, 1222 (1993).
[7] E. Fortin, S. Fafard, and A. Mysyrowicz, Phys. Rev. Lett. **70**, 3951 (1993).
[8] A. Mysyrowicz, E. Benson, and E. Fortin, Phys. Rev. Lett. **77**, 896 (1996).
[9] T. Goto, M. Y. Shen, S. Koyama, and T. Yokouchi, Phys. Rev. B **55**, 7609 (1997).
[10] M. Y. Shen, T. Yokouchi, S. Koyama, and T. Goto, Phys. Rev. B **56**, 13 066 (1997).
[11] K. E. O'Hara, Ph.D. thesis, University of Illinois at Urbana—Champaign, 1999.
[12] N. Peyghambarian, L. L. Chase, and A. Mysyrowicz, Phys. Rev. B **27**, 2325 (1983).
[13] M. Hasuo, N. Nagasawa, T. Itoh, and A. Mysyrowicz, Phys. Rev. Lett. **70**, 1303 (1993).
[14] G. A. Kopelevich, S. G. Tikhodeev, and N. A. Gippius, Zh. Éksp. Teor. Fiz. **109**, 2189 (1996) [JETP **82**, 1180 (1996)].
[15] S. G. Tikhodeev, Phys. Rev. Lett. **78**, 3225 (1997).
[16] M. H. Anderson, J. R. Ensher, M. R. Matthews, C. E. Weiman, and E. A. Cornell, Science **269**, 198 (1995).
[17] K. B. Davis, M. O. Mewes, M. R. Andrews, N. J. van Druten, D. S. Durfee, D. M. Kurn, and W. Ketterle, Phys. Rev. Lett. **75**, 3969 (1995).
[18] D. P. Trauernicht, J. P. Wolfe, and A. Mysyrowicz, Phys. Rev. B **34**, 2561 (1986).
[19] K. E. O'Hara, J. R. Gullingsrud, and J. P. Wolfe, Phys. Rev. B (to be published).
[20] J. S. Shumway and D. M. Ceperley, preprint, cond-mat/9907309.
[21] P. L. Gourley and J. P. Wolfe, Phys. Rev. B **24**, 5970 (1981).
[22] R. G. Waters, F. H. Pollak, R. H. Bruce, and H. Z. Cummins, Phys. Rev. B **21**, 1665 (1980).
[23] K. Reimann and K. Syassen, Phys. Rev. B **39**, 11 113 (1989).
[24] D. W. Snoke, D. Braun, and M. Cardona, Phys. Rev. B **44**, 2991 (1991).
[25] *Semiconductors, Intrinsic Properties of Group IV Elements and III-V, II-VI, and I-VII Compounds*, edited by O. Madelung and M. Schulz, Landolt-Börnstein, New Series, Group III, Vol. 22, Pt. a (Springer, Berlin, 1987).
[26] S. Timoshenko and J. N. Goodier, *Theory of Elasticity* (McGraw-Hill, New York, 1951), p. 375.
[27] A. Mysyrowicz, D. P. Trauernicht, J. P. Wolfe, and H.-R. Trebin, Phys. Rev. B **27**, 2562 (1983).
[28] See, e.g., G. D. Gilliland, D. J. Wolford, G. A. Northrop, M. S. Petrovic, T. F. Kuech, and J. A. Bradley, J. Vac. Sci. Technol. B **10**, 1959 (1992).
[29] D. W. Snoke, D. P. Trauernicht, and J. P. Wolfe, Phys. Rev. B **41**, 5266 (1990).
[30] P. D. Bloch and C. Schwab, Phys. Rev. Lett. **41**, 514 (1978).
[31] J. B. Grun, M. Sieskind, and S. Nikitine, J. Phys. Chem. Solids **19**, 189 (1961).
[32] G. M. Kavoulakis and G. Baym, Phys. Rev. B **54**, 16 625 (1996).
[33] P. Y. Yu and Y. R. Shen, Phys. Rev. Lett. **32**, 939 (1974); Phys. Rev. B **12**, 1377 (1975).